Editors' Suggestion | Featured in Physics

New Constraints on the Melting Temperature and Phase Stability of Shocked Iron up to 270 GPa Probed by Ultrafast X-Ray Absorption Spectroscopy

S. Balugani,[1,2] J. A. Hernandez,[1] N. Sévelin-Radiguet,[1] O. Mathon,[1] V. Recoules,[3] J. J. Kas,[4] D. E. Eakins,[5] H. Doyle,[6] A. Ravasio,[7] and R. Torchio[1]

[1]*European Synchrotron Radiation Facility (ESRF), 71 Avenue des Martyrs, Grenoble, CS 40220, 38043, France*
[2]*Institut Polytechnique de Paris, Route de Saclay, 91120 Palaiseau, France*
[3]*CEA/DAM DIF, F-91297 Arpajon Cedex, France*
[4]*Department of Physics, University of Washington, Seattle, Washington, USA*
[5]*Department of Engineering Science, University of Oxford, Parks Road, Oxford OX1 3PJ, United Kingdom*
[6]*First Light Fusion, Yarnton, England, United Kingdom*
[7]*LULI, CNRS, CEA, Sorbonne Université, École Polytechnique—Institut Polytechnique de Paris, Palaiseau, France*

(Received 27 May 2024; revised 4 September 2024; accepted 13 September 2024; published 18 December 2024)

Studying the properties and phase diagram of iron at high-pressure and high-temperature conditions has relevant implications for Earth's inner structure and dynamics and the temperature of the inner core boundary (ICB) at 330 GPa. Also, a hexagonal-closed packed to body-centered cubic (bcc) phase transition has been predicted by many theoretical works but observed only in a few experiments. The recent coupling of high-power laser with advanced x-ray sources from synchrotrons allows for novel approaches to address these issues. Here, we present a study on shock compressed iron up to 270 GPa and 5800 K probed by single-pulse (100 ps FWHM) x-ray absorption spectroscopy (XAS). Based on the analysis of the XAS spectra, we provide structural identification and bulk temperature measurements along the Hugoniot up to the melting. These results rule out the predicted transition to a high-temperature bcc phase and allow one to discriminate among existing equations of state models and melting curves. In particular, we report the first bulk temperature measurement in shock compressed iron on the melting plateau at 240(20) GPa and 5345 (600) K. The melting curve resulting from our work extrapolates to a temperature of 6202(514) K at 330 GPa and represents a refined upper bound for the ICB temperature.

DOI: 10.1103/PhysRevLett.133.254101

Iron is the primary component of Earth's and other terrestrial planets' cores. Its high-pressure properties and phase diagram are closely related to Earth's inner structure and dynamics [1]. Although Fe is alloyed with nickel and light elements in the core, the melting temperature of pure Fe provides an upper limit on the temperature at the boundary between the molten outer and solid inner core at 330 GPa. The crystallization of the inner core drives convection in the outer core, generating Earth's magnetic field. Iron's phase diagram has been extensively studied through static and dynamic compression [2–11]. At ambient temperature, Fe transforms from a body-centered cubic (bcc) structure to a hexagonal close-packed (hcp) structure at 13 GPa [12–14]. Below 100 GPa, Fe adopts a face-centered cubic structure before melting. The melting curve from static compression has been largely debated, but recent studies support a high-temperature melting curve of Fe, consistent with simulations and shock experiments [9,11,15–21]. Uncertainties remain regarding the melting temperature at core conditions (above 200 GPa). Some theoretical and experimental studies predict a high-temperature bcc phase [3,22–25], although many confirm the hcp phase at these conditions [6,9,11,18,26]. Above 200 GPa, most data come from shock and dynamic compression studies using plate impacts [19–21] and laser drivers [6–11]. Velocimetry-based hydrodynamic measurements have determined Fe's Hugoniot and indicated changes in sound speed at 200–260 GPa, typically interpreted as melting [27,28], though a solid-solid phase transition has also been suggested [27,29]. Recent advances in x-ray sources coupled with high-power lasers have enabled *in situ* bulk measurements under dynamic compression [30–34], providing insights into shocked Fe's structure. X-ray diffraction (XRD) studies show hcp iron persists alone up to 242 GPa [8–11], coexisting with molten Fe between 242 and 247 GPa [9]. Beyond this, only molten Fe exists on the Hugoniot [9]. Although some pyrometry measurements have been performed [19–21], temperature is generally not directly measured in these

experiments due to the low emissivity of Fe. Instead, it is typically inferred from thermodynamic calculations. Existing pyrometry studies have measured the thermal emission of shocked Fe at interfaces with various transparent crystalline windows (e.g., Al_2O_3, diamond, or LiF). However, these measurements depend on a thermal conduction model between the shocked Fe and the shocked window, leading to estimated errors of 10%–20% in the derived temperature [20]. Beyond providing information on the electronic and local atomic structure around absorber atoms, x-ray absorption spectroscopy (XAS) holds significant potential as a bulk temperature probe. The temperature (T) can be derived from the extended x-ray absorption fine structure (EXAFS) signal, where the oscillations are dampened by the Debye-Waller factor [35]. This approach has been employed at the OMEGA and National Ignition Facility laser facilities using a laser-induced x-ray source to study dynamically driven iron [36] and copper [37]. Additionally, single-pulse synchrotron XAS measurements of laser-shocked platinum and iron have been performed at advanced photon source dynamic compression sector [38] and ESRF [6]. Ping *et al.* [36] extracted bulk temperatures for shocked Fe at pressures below 150 GPa and for multishocked Fe up to 560 GPa in the hcp phase, although they did not reach the melting line. Torchio *et al.* [6] identified a melting signature in the XAS signal at an estimated shock pressure of 270 GPa but could determine temperatures for hcp Fe only up to 80 GPa. As a result, the melting temperature of shocked iron remains undetermined with this method.

In this study, we present single-pulse (100 ps) synchrotron K-edge XAS measurements of laser-driven shocked Fe at pressures ranging from 100(15) to 270(18) GPa. Our XAS data reveal that shocked Fe retains an hcp structure up to the melting line, with no evidence of a high-temperature bcc phase, consistent with recent XRD results [9,18]. Additionally, analysis of the EXAFS data provides bulk temperature measurements of shocked Fe along its solid Hugoniot up to the melting line, indicating a melting temperature of 5345(600) K at 240(20) GPa. These temperature measurements align with theoretical predictions [39,40] and extrapolations of high-temperature melting curves from static compression studies [2], providing important experimental constraints on the melting curve of Fe above 200 GPa.

The experiment was conducted at the European Synchrotron Radiation Facility (Grenoble, France) on the High Power Laser Facility (HPLF) at the ID24-ED beam line [33]. A schematic of the experimental setup is shown in Fig. 1. We used the HPLF drive laser to shock-compress multilayered targets consisting of a 25-μm-thick parylene-N ablator and a 3.5-μm-thick Fe sample deposited on an 80- or 100-μm-thick diamond window. A thin Al coating was applied to the laser side of the ablator to enhance laser-matter coupling. The ablation was achieved by focusing 10 ns flattop pulses at a wavelength of 1053 nm onto 250–100 μm diameter focal spots with hybrid phase plates. The drive laser energy was varied to probe the Hugoniot of

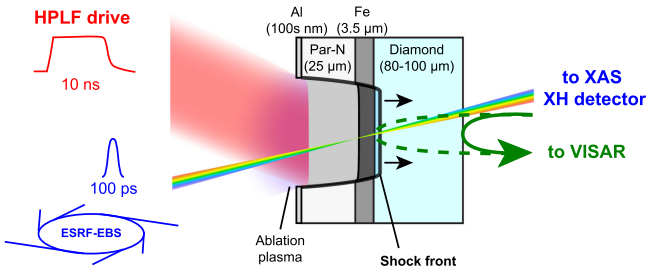

FIG. 1. Scheme of the experimental setup. The HPLF laser which drives the shock and the ESRF-Extremely Brilliant Source broadband x rays are focused on the target with ±15° angle relative to the normal of the target plane. The XAS absorbance spectrum μL is obtained by collecting the intensity of a single x-ray pulse transmitted through the sample during the shock $[I_1(E)]$ and by normalizing it to a reference intensity profile without sample $[I_0(E)]$.

Fe across the pressure range of 100(15)–270(18) GPa. A line-imaging velocity interferometer system for any reflector (VISAR) operating at 532 nm was employed to measure shock timings as it entered and exited the diamond window, as well as the diamond's free surface velocity. These data were used to determine pressure values in the Fe layer via ESTHER hydrodynamic simulations [41] (detailed in Supplemental Material [42]).

Time-resolved single-bunch XAS was performed at the Fe K edge (7.112 keV) using an energy-dispersive setup in the 16-bunch timing mode of the ESRF. The ID24-ED pink x-ray beam was dispersed and focused onto the sample to a 6 μm × 6 μm spot using an elliptically bent Si(111) crystal (polychromator) [33]. The beam then diverged and was captured by a 1D position-sensitive detector (XH) [49], enabling collection of a full XAS spectrum in a single 100 ps x-ray pulse synchronized with the shock, with an energy resolution of 1 eV. The delay between the drive laser and the x-ray single bunch was precisely tuned to capture the fully shocked Fe when the shock reached the Fe-diamond interface. Potential target preheating by x-rays from the coronal plasma was ruled out by verifying the XAS spectrum at early times, before the shock wave had reached the Fe layer (see Supplemental Material [42]).

Figure 2(a) shows the normalized Fe K-edge XAS spectra collected at increasing pressure and temperature conditions along the Hugoniot curve. The black-colored spectrum of unshocked Fe corresponds to the ambient bcc phase. For the shock-driven spectra, the pressure in Fe was derived using an experimental-theoretical approach where the 1D-hydrodynamic ESTHER simulations [41] were combined with the experimental travel times from VISAR and laser pulse shape (see Supplemental Material [42]). The high data quality allows to detect fine changes in both the x-ray absorption near edge structure (XANES) and EXAFS regions. These changes are related to structural transitions (XANES and EXAFS modification), lattice

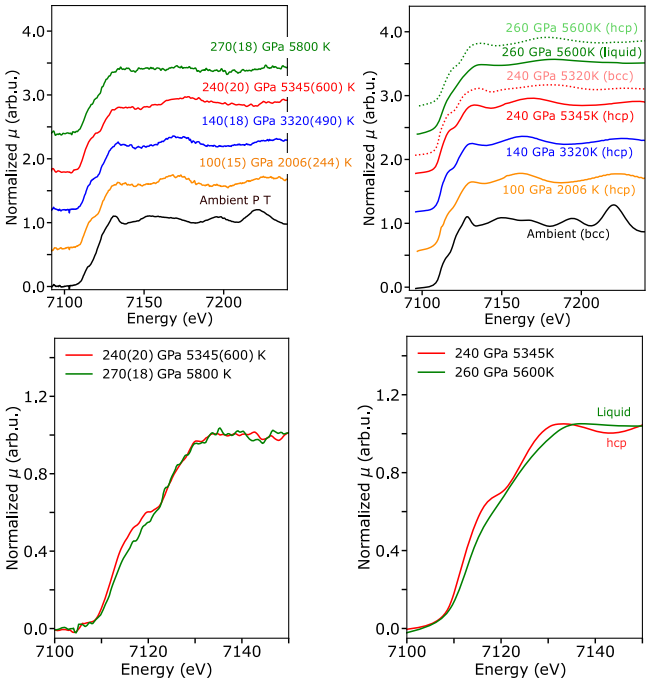

FIG. 2. Top left: normalized single-pulse K-edge XAS spectra of iron collected under laser-driven shock compression along the Hugoniot curve. The spectra are vertically shifted and ordered for increasing pressure and temperature for a better visualization. The ambient spectrum is the average of ten acquisitions, whereas the spectra at shocked conditions are single bunch acquisitions (100 ps). The error propagation on the P-T conditions is described in Supplemental Material [42]. Top right: simulated K-edge XAS spectra of iron at the similar conditions of pressure and temperature done with FEFF 10 code and combined with density-functional theory–molecular dynamics (DFT-MD) Vienna *ab initio* simulation (VASP) package code for the liquid (green) and the solid hcp (dotted green) at 260 GPa and 5600 K. The dotted spectrum at 240 GPa simulates the bcc phase instead of hcp at the same conditions. Bottom: XANES region of the spectra at the two highest pressure experimental points (left) and simulated ones (right).

compression (EXAFS oscillations shifted to higher energy), and thermal disorder (broadening of EXAFS oscillations).

XAS spectra at 100(15) and 140(18) GPa have characteristic fingerprints of hcp Fe. This is confirmed by comparison with static compression data [50] and by simulations of XAS spectra from Fe hcp structure using FEFF10 software [43,44,51] [Fig. 2(b) and see Supplemental Material [42]]. The spectrum at 240(20) GPa is also compatible with the hcp structure, but it shows partial flattening of the postedge at about 7130 eV. In the spectrum at 270(18) GPa, the edge shape also flattens and EXAFS oscillations are lost, see bottom panels in Fig. 2. These changes have been previously identified with occurrence of melting in laser-heated DAC experiments [5,45,52] in milder conditions (around 100 GPa).

Taking advantage of EXAFS sensitivity to thermal disorder, we extracted the temperature from the fit of the EXAFS signal χ performed with the ARTEMIS package [46]. In the harmonic approximation, the EXAFS equation for polycrystalline samples reads [53]

$$\chi(k) = S_0^2 \sum_i N_i \frac{f_i(k)}{kR_i^2} \sin[2kR_i + \delta_i(k)] e^{-2R_i/\lambda_i(k)} e^{-2k^2\sigma_i^2}, \tag{1}$$

where k is the photoelectron wave number and S_0^2 is an amplitude reduction factor that takes into account the relaxation of the absorbing atom due to the presence of a core hole. Here, i, N_i, $f_i(k)$, $\delta_i(k)$, and $\lambda_i(k)$ represent the scattering path index, path degeneracy, effective scattering amplitude, phase shift, and inelastic mean free path, respectively. For a given structure, these parameters are calculated by FEFF, while the half-path lengths (R_i) and the mean-squared relative displacements (σ_i) are fitted [53]. The term $e^{-2k^2\sigma_i^2}$ is the Debye-Waller factor and acts as a dampening term for the EXAFS oscillations. We first performed the EXAFS fit of unshocked bcc spectrum in order to fix the amplitude reduction factor S_0^2. Then, we performed the EXAFS fits of all shocked spectra up to 240 (20) GPa considering a hcp structure and determined the temperature from the mean-squared relative displacements using the correlated Debye and the correlated Einstein models. We chose to show the result from the Debye model as the fit quality was better, but we included an error that was covering also the result obtained from applying the Einstein model (Supplemental Material [42]). Debye temperatures T_D were taken from Sharma [47], and the details of the fits are reported in Supplemental Material [42]. We checked for the anharmonic contribution to the temperature as anharmonic effects can start to play a non-negligible role at $T/T_D > 5$ [36]. The anharmonic correction given by the third-order coefficient of the Taylor expansion for the Debye-Waller factor was considered for the highest-pressure highest-temperature spectrum we analyzed at 240 (20) GPa and found to be negligible within the temperature uncertainty. The temperatures obtained with this approach are provided in Fig. 3 and in Supplemental Material [42]. The two lowest pressures 100(15) and 140(18) GPa lie within the solid region of the phase diagram with temperature of 2006(244) and 3320(490) K, respectively. At these conditions, existing experimental Hugoniot data and models are all in line, and our measurements confirm this trend. At higher pressures, though, the models significantly diverge, predicting different melting temperatures. Our results at 240(20) and 270(18) GPa are key to discriminate between these models. The comparison with FEFF simulations at the measured conditions (Fig. 2, bottom panels) indicate that these two spectra are compatible with onset and predominant melting. Indeed, the XAS spectrum acquired at 240(20) GPa is similar to a solid hcp phase, but the postedge feature around 7130 eV is flatter and closer

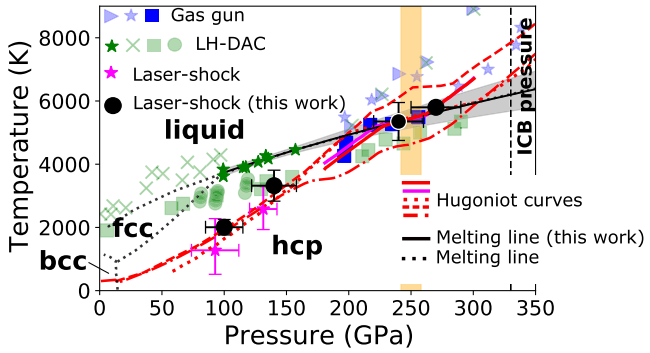

FIG. 3. Phase diagram of iron at high pressure and high temperature. The black dots show the conditions investigated in this study, with the white-edge dot corresponding to our shot on the melting plateau. The black solid line represents the Simon-Glatzel fit of Anzellini *et al.* [2] data together with our melting point at 240(20) GPa, and the corresponding 1σ error is shown by the gray area. fcc phase boundaries are shown by the black dotted line [2]. The black dashed line indicates the ICB pressure at 330 GPa. The dashed red and the dot-dashed red curves correspond to the Bushman-Lomonosov-Fortov [60] and SESAME2150 [29] Hugoniot curves, respectively. The dotted red line marks the *ab initio* Hugoniot of Bouchet *et al.* [17]. The recent Hugoniot curves proposed by Benedict *et al.* and Wu *et al.* [15,16] are illustrated in pink and red solid lines, respectively. Blue and green markers show results from gas-gun [19–21] and static compression data [54,61,62] experiments, respectively. Pink stars show EXAFS single shock compression data from [36]. The orange band indicates the pressure extent of the melting plateau along the Hugoniot reported by [9,18]. The temperature of our highest pressure data point could not be determined by EXAFS and was estimated from Benedict *et al.* [15] EOS.

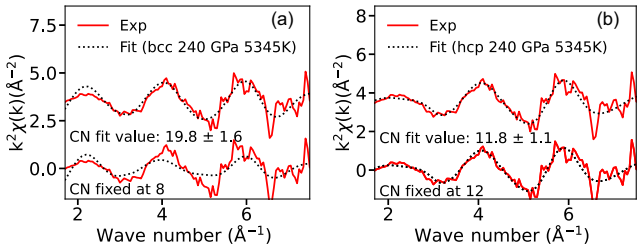

FIG. 4. k^2-weighted EXAFS oscillations of Fe K edge. Solid lines correspond to experimental data, while the dotted lines refer to the theoretical curves. (a) Shows the experimental data at 240 GPa together with the EXAFS fit using a bcc cluster of atoms for a CN fixed to 8 (lower curve) and for a coordination number left free (upper curve). (b) Shows the same experimental data fit using a hcp cluster of atoms with the coordination number fixed at 12 (lower curve), characteristic of the first shell of an hcp structure and then left free (upper curve).

to a liquid shape. The XAS spectrum at 270(18) GPa shows an important flattening of the edge slope and dampening of the EXAFS oscillations as expected for a liquid phase. These observations are in very good agreement with recent laser-driven shock-compression experiments coupled to *in situ* XRD, where the melting plateau has been observed between 241.5(3) and 258(8) GPa [9,18]. The EXAFS analysis of the shot at 240(20) GPa provides the first bulk temperature determination on the melting plateau of 5345 (600) K. This melting point is in agreement with the extrapolation of lower pressure melting data from static compression experiments from Ref. [2] and from ramp-compression experiments where the temperature was estimated based on thermodynamic calculations [11]. It is worth noting that our data disagree with the lower temperature melting curve of Sinmyo, Hirose, and Ohishi obtained from static compression and internal resistive heating [54]. According to this study, we should already have reached the melting plateau at 140(18) GPa, which we did not. In addition, our data validate the equation of state model of Benedict *et al.* and Wu *et al.* [15,16], which was then used to estimate the temperature corresponding to our shot at 270(18) GPa at 5800 K [Figs. 2(a) and 3]. To further anchor the melting curve of hcp iron, we used the Simon-Glatzel semiempirical law to extrapolate the melting temperature at 330 GPa, the pressure of the Earth inner core boundary (ICB). We fitted the equation to a dataset composed of the XRD data from static compression studies [2] covering the pressure range below 160 GPa—where melting was observed—together with our point at 240(20) GPa (black dot with white edge in Fig. 3). More information on the fit is provided in Supplemental Material [42]. We obtain a melting temperature of 6202(514) K at 1σ uncertainty for pure Fe at the ICB pressure. This represents an upper bound for the temperature at the ICB, since the outer core includes light elements that are likely decreasing the melting temperature [55]. Last, our data exclude the presence of a hcp-bcc transition before melting, which has been predicted by several theoretical studies [22,24,56–59] but supported by only a few experimental observations [3,25]. In Fig. 2(b), a simulated bcc spectrum at 240 GPa and 5345 K is shown (dotted curve) and compared with a simulated hcp spectrum at similar conditions. The dotted curve was produced using a bcc cluster of atoms in the compressed and hot state modeled with FEFF. Qualitatively, the experimental spectrum is better reproduced by the hcp structure, and the simulated bcc spectrum shows smaller and shifted oscillations in the EXAFS region compared to the measurement. Moreover, we demonstrate the bcc phase cannot be used to obtain a consistent fit to the EXAFS. Figure 4(a) shows two fits of the EXAFS measured at 240 (20) GPa, both considering a bcc structure, but one with the coordination number (CN) fixed at 8 (eight atoms degeneracy in the first coordination shell) as expected for a bcc structure (bottom) and another one where the CN was a free parameter of the fit (top). Fixing the CN does not result in a good fit, and, when let free, CN converges to 19.8(1.6), which is inconsistent with the expected value of 8.

In contrast, when applying the same procedure with a hcp structure, we obtain two equally good fits and the free CN converges toward 11.8(1.1), close to the expected value of 12. Again, these results confirm recent XRD measurements showing only the hcp phase is observed under shock up to melting [9,18].

In conclusion, we present single-pulse (≈100 ps) K-edge XAS data on laser-driven shock compressed iron up to shock melting at 270 (18) GPa and 5800 K. First, we rule out the formation of a high-temperature bcc phase before melting along the Hugoniot around 240 GPa. Then, we constrain further the extension of the melting plateau by observing the onset melting and molten iron, respectively, at 240(20) and 270(18) GPa, showing that the recent multiphase equation of states in Refs. [15,16] are the most accurate, while the equation of state (EOS) in Ref. [17] overestimates the extension of melting plateau. Most importantly, we report the first bulk temperature measurement on the melting plateau at 240(20) GPa and 5345 (600) K, which unambiguously confirms the extrapolation of the high-temperature melting measurements in Ref. [2]. Considering the Anzellini *et al.* dataset and our melting point, we provide a new melting line of hcp Fe which gives a new upper bound for the ICB temperature of 6202(514) K at 330 GPa.

Acknowledgments—We thank the ESRF for providing beam time for the scientific projects IH-MA-271, Florent Occelli for the help during the experiment, and Silvia Boccato and Clément Bonnet for the discussions. This project has received funding from the European Union's Horizon 2020 research and innovation program under the Marie Skłodowska-Curie Grant Agreement No. 847439 (InnovaXN). J. J. K. is supported by the Theory Institute for Materials and Energy Spectroscopies (TIMES) at SLAC, which is funded by the U.S. Department of Energy, Office of Basic Energy Sciences, Division of Materials, Sciences and Engineering, under Contract No. DE AC02-76SF0051. We also acknowledge the support of LULI laboratory for the loaning of their probe laser, especially S. Baton, A. Benuzzi, and T. Vinci.

[1] F. Birch, Elasticity and constitution of the Earth's interior, J. Geophys. Res. **57**, 227 (1952).
[2] S. Anzellini, A. Dewaele, M. Mezouar, P. Loubeyre, and G. Morard, Melting of iron at Earth's inner core boundary based on fast x-ray diffraction, Science **340**, 464 (2013).
[3] L. Dubrovinsky, N. Dubrovinskaia, and V. Prakapenka, En las condiciones del nucleo de la tierra,? tiene el hierro una estructura hcp?, Fisica de la Tierra **23**, 73 (2011).
[4] S. Tateno, K. Hirose, Y. Ohishi, and Y. Tatsumi, The structure of iron in Earth's inner core, Science **330**, 359 (2010).
[5] G. Morard, S. Boccato, A. D. Rosa, S. Anzellini, F. Miozzi, L. Henry, G. Garbarino, M. Mezouar, M. Harmand, F. Guyot *et al.*, Solving controversies on the iron phase diagram under high pressure, Geophys. Res. Lett. **45**, 11 (2018).
[6] R. Torchio, F. Occelli, O. Mathon, A. Sollier, E. Lescoute, L. Videau, T. Vinci, A. Benuzzi-Mounaix, J. Headspith, W. Helsby *et al.*, Probing local and electronic structure in warm dense matter: Single pulse synchrotron x-ray absorption spectroscopy on shocked Fe, Sci. Rep. **6**, 26402 (2016).
[7] M. Harmand, A. Ravasio, S. Mazevet, J. Bouchet, A. Denoeud, F. Dorchies, Y. Feng, C. Fourment, E. Galtier, J. Gaudin *et al.*, X-ray absorption spectroscopy of iron at multimegabar pressures in laser shock experiments, Phys. Rev. B **92**, 024108 (2015).
[8] A. Denoeud, N. Ozaki, A. Benuzzi-Mounaix, H. Uranishi, Y. Kondo, R. Kodama, E. Brambrink, A. Ravasio, M. Bocoum, J.-M. Boudenne *et al.*, Dynamic x-ray diffraction observation of shocked solid iron up to 170 GPa, Proc. Natl. Acad. Sci. U.S.A. **113**, 7745 (2016).
[9] S. J. Turneaure, S. M. Sharma, and Y. M. Gupta, Crystal structure and melting of Fe shock compressed to 273 GPa: In situ x-ray diffraction, Phys. Rev. Lett. **125**, 215702 (2020).
[10] S. White, B. Kettle, J. Vorberger, C. L. S. Lewis, S. Glenzer, E. Gamboa, B. Nagler, F. Tavella, H. J. Lee, C. D. Murphy, D. O. Gericke, and D. Riley, Time-dependent effects in melting and phase change for laser-shocked iron, Phys. Rev. Res. **2**, 033366 (2020).
[11] R. G. Kraus, R. J. Hemley, S. J. Ali, J. L. Belof, L. X. Benedict, J. Bernier, D. Braun, R. Cohen, G. W. Collins, F. Coppari *et al.*, Measuring the melting curve of iron at super-earth core conditions, Science **375**, 202 (2022).
[12] D. Bancroft, E. L. Peterson, and S. Minshall, Polymorphism of iron at high pressure, J. Appl. Phys. **27**, 291 (1956).
[13] D. H. Kalantar, J. F. Belak, G. W. Collins, J. D. Colvin, H. M. Davies, J. H. Eggert, T. C. Germann, J. Hawreliak, B. L. Holian, K. Kadau, P. S. Lomdahl, H. E. Lorenzana, M. A. Meyers, K. Rosolankova, M. S. Schneider, J. Sheppard, J. S. Stolken, and J. S. Wark, Direct observation of the $\alpha - \varepsilon$ transition in shock-compressed iron via nanosecond x-ray diffraction, Phys. Rev. Lett. **95**, 075502 (2005).
[14] J. C. Jamieson and A. Lawson, X-ray diffraction studies in the 100 kilobar pressure range, J. Appl. Phys. **33**, 776 (1962).
[15] L. Benedict, R. Kraus, S. Hamel, and J. Belof, A Limited-Ranged Two-Phase Iron Equation of State Model, Technical Report No. LLNL-TR-831239, Lawrence Livermore National Lab, Livermore, CA, 2022, https://doi.org/10.2172/1843135.
[16] C. J. Wu, L. X. Benedict, P. C. Myint, S. Hamel, C. J. Prisbrey, and J. R. Leek, Wide-ranged multiphase equation of state for iron and model variations addressing uncertainties in high-pressure melting, Phys. Rev. B **108**, 014102 (2023).
[17] J. Bouchet, S. Mazevet, G. Morard, F. Guyot, and R. Musella, *Ab initio* equation of state of iron up to 1500 GPa, Phys. Rev. B **87**, 094102 (2013).
[18] S. Singh, R. Briggs, M. G. Gorman, L. X. Benedict, C. J. Wu, A. L. Coleman, F. Coppari, A. Fernandez-Panella, C. McGuire, M. Sims *et al.*, Structural study of hcp and liquid iron under shock compression up to 275 GPa, Phys. Rev. B **108**, 184104 (2023).

[19] J. D. Bass, B. Svendsen, and T. J. Ahrens, The temperature of shock compressed iron, High-Pressure Res. Miner. Phys. **39**, 393 (1987).
[20] C. S. Yoo, N. C. Holmes, M. Ross, D. J. Webb, and C. Pike, Shock temperatures and melting of iron at earth core conditions, Phys. Rev. Lett. **70**, 3931 (1993).
[21] J. Li, Q. Wu, J. Li, T. Xue, Y. Tan, X. Zhou, Y. Zhang, Z. Xiong, Z. Gao, and T. Sekine, Shock melting curve of iron: A consensus on the temperature at the Earth's inner core boundary, Geophys. Res. Lett. **47**, e2020GL087758 (2020).
[22] A. B. Belonoshko, J. Fu, and G. Smirnov, Free energies of iron phases at high pressure and temperature: Molecular dynamics study, Phys. Rev. B **104**, 104103 (2021).
[23] A. B. Belonoshko, S. I. Simak, W. Olovsson, and O. Y. Vekilova, Elastic properties of body-centered cubic iron in Earth's inner core, Phys. Rev. B **105**, L180102 (2022).
[24] M. Ghosh, S. Zhang, L. Hu, and S. Hu, Cooperative diffusion in body-centered cubic iron in earth and super-earths' inner core conditions, J. Phys. Condens. Matter **35**, 154002 (2023).
[25] R. Hrubiak, Y. Meng, and G. Shen, Experimental evidence of a body centered cubic iron at the Earth's core condition, arXiv:1804.05109.
[26] Y. Zhang, Y. Wang, Y. Huang, J. Wang, Z. Liang, L. Hao, Z. Gao, J. Li, Q. Wu, H. Zhang *et al.*, Collective motion in hcp-Fe at Earth's inner core conditions, Proc. Natl. Acad. Sci. U.S.A. **120**, e2309952120 (2023).
[27] J. M. Brown and R. G. McQueen, Phase transitions, Grüneisen parameter, and elasticity for shocked iron between 77 GPa and 400 GPa, J. Geophys. Res. **91**, 7485 (1986).
[28] J. H. Nguyen and N. C. Holmes, Melting of iron at the physical conditions of the Earth's core, Nature (London) **427**, 339 (2004).
[29] G. Kerley, Multiphase equation of state for iron, SANDIA, Report No. SAND93–0027, 1993, https://doi.org/10.2172/6345571.
[30] M. Gorman, D. McGonegle, R. Smith, S. Singh, T. Jenkins, R. McWilliams, B. Albertazzi, S. Ali, L. Antonelli, M. Armstrong *et al.*, Shock compression experiments using the DIPOLE 100-x laser on the high energy density instrument at the European X-ray Free Electron Laser: Quantitative structural analysis of liquid Sn, J. Appl. Phys. **135**, 165902 (2024).
[31] R. Briggs, F. Coppari, M. G. Gorman, R. F. Smith, S. J. Tracy, A. L. Coleman, A. Fernandez-Pañella, M. Millot, J. H. Eggert, and D. E. Fratanduono, Measurement of body-centered cubic gold and melting under shock compression, Phys. Rev. Lett. **123**, 045701 (2019).
[32] J. Rygg, R. Smith, A. Lazicki, D. Braun, D. Fratanduono, R. Kraus, J. McNaney, D. Swift, C. Wehrenberg, F. Coppari *et al.*, X-ray diffraction at the National Ignition Facility, Rev. Sci. Instrum. **91**, 043902 (2020).
[33] J.-A. Hernandez, N. Sévelin-Radiguet, R. Torchio, S. Balugani, A. Dwivedi, G. Berruyer, D. Bugnazet, S. Chazalette, C. Clavel, D. Lorphévret *et al.*, The high power laser facility at beamline ID24-ED at the ESRF, High Press. Res. **44**, 372 (2024).
[34] Y. Ping and F. Coppari, Laser shock XAFS studies at omega facility, High Press. Res. **36**, 303 (2016).
[35] E. Sevillano, H. Meuth, and J. J. Rehr, Extended x-ray absorption fine structure Debye-Waller factors. I. Monatomic crystals, Phys. Rev. B **20**, 4908 (1979).
[36] Y. Ping, F. Coppari, D. G. Hicks, B. Yaakobi, D. E. Fratanduono, S. Hamel, J. H. Eggert, J. R. Rygg, R. F. Smith, D. C. Swift, D. G. Braun, T. R. Boehly, and G. W. Collins, Solid iron compressed up to 560 GPa, Phys. Rev. Lett. **111**, 065501 (2013).
[37] H. Sio, A. Krygier, D. Braun, R. Rudd, S. Bonev, F. Coppari, M. Millot, D. Fratanduono, N. Bhandarkar, M. Bitter *et al.*, Extended x-ray absorption fine structure of dynamically-compressed copper up to 1 terapascal, Nat. Commun. **14**, 7046 (2023).
[38] S. J. Turneaure and P. Das, Vibrational response and temperature of shock-compressed Pt: In situ extended x-ray absorption fine structure measurements to 325 GPa, Phys. Rev. B **105**, 174103 (2022).
[39] T. Sun, J. P. Brodholt, Y. Li, and L. Vočadlo, Melting properties from *ab initio* free energy calculations: Iron at the Earth's inner-core boundary, Phys. Rev. B **98**, 224301 (2018).
[40] D. Alfe, Temperature of the inner-core boundary of the earth: Melting of iron at high pressure from first-principles coexistence simulations, Phys. Rev. B **79**, 060101(R) (2009).
[41] S. Bardy, B. Aubert, T. Bergara, L. Berthe, P. Combis, D. H'bert, E. Lescoute, Y. Rouchausse, and L. Videau, Development of a numerical code for laser-induced shock waves applications, Opt. Laser Technol. **124**, 105983 (2020).
[42] See Supplemental Material at http://link.aps.org/supplemental/10.1103/PhysRevLett.133.254101, which includes Refs. [2,9,11,35,41,43–48], for additional information about the experimental methods and a detailed discussion of the numerical simulations.
[43] J. Kas, F. Vila, C. Pemmaraju, T. Tan, and J. Rehr, Advanced calculations of x-ray spectroscopies with FEFF10 and corvus, J. Synchrotron Radiat. **28**, 1801 (2021).
[44] J. J. Rehr, J. J. Kas, M. P. Prange, A. P. Sorini, Y. Takimoto, and F. Vila, *Ab initio* theory and calculations of x-ray spectra, C.R. Phys. **10**, 548 (2009).
[45] S. Boccato, Local structure of liquid 3d metals under extreme conditions of pressure and temperature, Ph.D. thesis, Université Grenoble Alpes, 2017.
[46] B. Ravel and M. Newville, ATHENA, ARTEMIS, HEPHAESTUS: Data analysis for x-ray absorption spectroscopy using ifeffit, J. Synchrotron Radiat. **12**, 537 (2005).
[47] S. Sharma, Debye temperature of hcp iron at extreme compression, Solid State Commun. **149**, 2207 (2009).
[48] C. Marini, F. Occelli, O. Mathon, R. Torchio, V. Recoules, S. Pascarelli, and P. Loubeyre, A microsecond time resolved x-ray absorption near edge structure synchrotron study of phase transitions in Fe undergoing ramp heating at high pressure, J. Appl. Phys. **115** (2014).
[49] M. Borri, C. Cohen, J. Groves, W. Helsby, O. Mathon, L. McNicholl, N. Sévelin-Radiguet, R. Torchio, and M. Zuvic, Prototyping experience with Ge micro-strip sensors for EDXAS experiments, Nucl. Instrum. Methods Phys. Res., Sect. A **1017**, 165800 (2021).
[50] O. Mathon, F. Baudelet, J. P. Itié, A. Polian, M. d'Astuto, J. C. Chervin, and S. Pascarelli, Dynamics of the magnetic and structural $\alpha - \epsilon$ phase transition in iron, Phys. Rev. Lett. **93**, 255503 (2004).

[51] T. S. Tan, J. J. Kas, and J. J. Rehr, Real-space Green's function approach for x-ray spectra at high temperature, Phys. Rev. B **104**, 035144 (2021).

[52] S. Boccato, R. Torchio, I. Kantor, G. Morard, S. Anzellini, R. Giampaoli, R. Briggs, A. Smareglia, T. Irifune, and S. Pascarelli, The melting curve of nickel up to 100 GPa explored by XAS, J. Geophys. Res. **122**, 9921 (2017).

[53] J. J. Rehr and R. C. Albers, Theoretical approaches to x-ray absorption fine structure, Rev. Mod. Phys. **72**, 621 (2000).

[54] R. Sinmyo, K. Hirose, and Y. Ohishi, Melting curve of iron to 290 GPa determined in a resistance-heated diamond-anvil cell, Earth Planet. Sci. Lett. **510**, 45 (2019).

[55] G. Morard, D. Andrault, D. Antonangeli, Y. Nakajima, A. Auzende, E. Boulard, S. Cervera, A. Clark, O. Lord, J. Siebert, V. Svitlyk, G. Garbarino, and M. Mezouar, Fe–FeO and Fe–Fe3C melting relations at Earth's core–mantle boundary conditions: Implications for a volatile-rich or oxygen-rich core, Earth Planet. Sci. Lett. **473**, 94 (2017).

[56] M. Matsui and O. L. Anderson, The case for a body-centered cubic phase (α') for iron at inner core conditions, Phys. Earth Planet. Inter. **103**, 55 (1997).

[57] L. Vočadlo, I. G. Wood, M. J. Gillan, J. Brodholt, D. P. Dobson, G. D. Price, and D. Alfè, The stability of bcc-Fe at high pressures and temperatures with respect to tetragonal strain, Phys. Earth Planet. Inter. **170**, 52 (2008).

[58] M. J. Brown, The equation of state of iron to 450 GPa: Another high pressure solid phase?, Geophys. Res. Lett. **28**, 4339 (2001).

[59] A. B. Belonoshko, P. I. Dorogokupets, B. Johansson, S. K. Saxena, and L. Koči, *Ab initio* equation of state for the body-centered-cubic phase of iron at high pressure and temperature, Phys. Rev. B **78**, 104107 (2008).

[60] I. Lomonosov, A. V. Bushman, and V. E. Fortov, Equations of state for metals at high energy densities, AIP Conf. Proc. **309**, 117 (1994).

[61] Q. Williams, R. Jeanloz, J. Bass, B. Svendsen, and T. J. Ahrens, The melting curve of iron to 250 gigapascals: A constraint on the temperature at Earth's center, Science **236**, 181 (1987).

[62] G. Aquilanti, A. Trapananti, A. Karandikar, I. Kantor, C. Marini, O. Mathon, S. Pascarelli, and R. Boehler, Melting of iron determined by x-ray absorption spectroscopy to 100 GPa, Proc. Natl. Acad. Sci. U.S.A. **112**, 12042 (2015).